Combining a ground-based UV network with satellite maps: A case study for Germany

Barbara Klotz[1], Verena Schenzinger[1], Michael Schwarzmann[1], and Axel Kreuter[1,2]

[1]Institute of Biomedical Physics, Medical University Innsbruck, Innsbruck, Austria
[2]LuftBlick OG, Innsbruck, Austria

Correspondence: Barbara Klotz (barbara.klotz@i-med.ac.at)

Abstract. A study for the comprehensive information of current UV exposure for the area of Germany, based on the method for near real time calculation of UV Index maps used in the framework of the Austrian UV Monitoring Network, is presented. For the area of Germany about 22.000 surface UV Index maps were calculated for the year 2022 via the radiative transfer model libRadtran by incorporating daily forecast data for ozone, albedo and aerosols from the Copernicus Atmospheric Monitoring Service and taking into account cloud information gathered from SEVIRI data of Meteosat Second Generation in the form of a cloud modification factor. Ground-based measurements of 17 stations of the German Solar Monitoring Network were then compared to the modelled maps. For most stations the correlation coefficient between measured and modelled UV Index (UVI) is above 0.92 and the mean difference of modelled UVI to measured UVI is smaller than 0.5 UVI. The modelling of the UVI at the high mountain station Schneefernerhaus is associated with higher uncertainties (correlation coefficient 0.85 and mean UVI difference 0.6 UVI) due to the small-scale topography with spatially highly variable albedo and clouds. Moreover, case studies for specific locations with respect to cloud conditions and topography are discussed, as well as a case study of the combination of ground-based measurements and modelled UVI maps in form of spatial correction factors.

1 Introduction

Depending on the level of exposure, solar ultraviolet (UV) radiation has beneficial as well as damaging effects on human health. Moderate exposure has a positive impact on blood pressure and mental health (Juzeniene et al. (2011)) and it is the main driver for the synthesis of vitamin D in human skin (Webb and Engelsen (2006), Webb et al. (2011)), which is associated with an improved immune function. Overexposure to UV radiation on the other hand can lead to adverse effects like sunburn (erythema), eye damage (photokeratitis, cataract) and skin cancer (Lucas et al. (2006), Juzeniene et al. (2011)).

With the discovery of the Antarctic ozone hole in 1985, growing concerns about rising ultraviolet (UV) levels on the earth's surface led to the establishment of monitoring networks. Although ground-based measurements provide the actual radiation levels on the earth's surface, their spatial range of validity is confined to the surrounding of the measurement station since local conditions of cloud cover, ozone, albedo and aerosol amount have a strong impact on the measured radiation. On the other hand, satellite-based imagery offers comprehensive coverage of geographic areas. However, their acquisition is not continuous, and the granularity of the resulting data is depending on the spatial, spectral and radiometric resolution of the measurement device

25 onboard the satellite. Moreover, with this technique it is not possible to measure the UV radiation at the earth's surface directly, but there are methods of combining radiative transfer modelling with satellite data to calculate UV maps (Verdebout (2000), Schallhart et al. (2008), Kosmopoulos et al. (2021), Schenzinger et al. (2023)).

Nowadays the method described in Schenzinger et al. (2023) is in routine use in the framework of the Austrian UV Monitoring Network to calculate UV Index (UVI, see definition in WHO/WMO (2002)) maps of Europe every 15 minutes (see

30 www.uv-index.at).

In the present study the same method is applied to the area of Germany and the calculated UV Index maps are compared to measurements of 17 stations of the German Solar Monitoring Network for the year 2022. The peculiarities of the statistics of the UVI difference of modelled to measured UVI for clear, cloudy and all sky conditions are discussed and case studies of specific locations with respect to cloud conditions and topography are presented. For cloudy conditions as well as locations with highly

35 variable topography (station Schneefernerhaus) the agreement between model and measurement deteriorates in comparison to the clear sky case. This is mainly due to the comparison of a point measurement at the ground, which is influenced by very local conditions of e.g. clouds and albedo, with UV Index map values, whose modelling is based on input parameters obtained as averages over pixel sizes. So the objective is to explore opportunities for combining ground-based measurements with satellite-derived maps, thereby benefiting of the high accuracy of ground measurements alongside the extensive coverage

40 provided by satellite data. A case study of a correction factor map, gained from the ratio of measured to modelled UV Index, is discussed, highlighting the problems involved in combining both datasets.

2 Method

The procedure of producing UV Index maps used for this study is described and discussed in detail in Schenzinger et al. (2023), so here a summary is provided.

45 First a lookup table (LUT) of erythemal irradiance at the surface for clear sky conditions is pre-calculated with the sdisort solver of the radiative transfer model libRadtran (Mayer and Kylling (2005), Emde et al. (2016)). The entries of the LUT are solar elevation, height above sea level (m a.s.l.), total ozone column, albedo and Angstrom β.

Then clear sky UV Index maps for the area of Germany are extracted from the LUT by providing day-to-day forecasts of ozone, albedo and aerosol optical depth (AOD at 550 nm) from the Copernicus Atmospheric Monitoring Service (CAMS)

50 global model forecast (CAMS (2021)), where Angstrom β is calculated from the AOD with Angstrom α 1.4. For the spatial distribution of the height a.s.l. the digital elevation model GTOPO30 (Gesch et al. (1999)) is used and the solar elevation is calculated to match the timing of satellite cloud information from the SEVIRI instrument onboard the MSG (Meteosat Second Generation) satellite.

In order to adapt the clear sky model maps to cloudy conditions, SEVIRI imagery is utilized to derive cloud modification

55 factors (CMF) for the area of Germany every 15 minutes. The process of calculating a CMF is only done for pixels that are considered to be cloudy by the cloud mask obtained from the MSG Meteorological Products Extraction Facility (EUMETSAT (2015)). Then satellite images at 600 nm recorded by the SEVIRI instrument (EUMETSAT (2017)) together with a very simple

min-max scaling of the irradiance at the top of the atmosphere are used to estimate the CMF, which is a number between zero and one (zero meaning that there is an overcast sky with no radiation passing through and one describing a cloudless sky). Finally, the clear sky model maps are multiplied with the corresponding CMF to obtain near real time UV Index maps of Germany. A discussion of the uncertainties involved for this method is given in Schenzinger et al. (2023).

For this study almost 22.000 UV Index maps were calculated for various solar elevations and throughout the entire year of 2022, by incorporating CAMS forecasted data and satellite cloud information. Then the modelled values were compared with ground-based measurements of 17 sites of the German Solar Monitoring Network.

2.1 Ground measurements

A comparison of the modelled UV Index maps with ground measurements of the German Solar Monitoring Network for the year 2022 was performed. Currently, the German Solar Monitoring Network comprises 41 measurement sites. Prior to analysis, all ground data underwent preprocessing and quality control conducted by the German Federal Office for Radiation Protection. Finally measurements from 17 locations were selected (see Fig. 1) to cover the area of Germany from the sea in the north to the alpine region in the south, thereby also covering different altitudes. Most of the stations (14) are located below 600 m a.s.l. (green markers in Fig. 1), two of them are at a height of around 1000 m a.s.l. (orange markers) and the high alpine station at Schneefernerhaus is located below the summit of mount Zugspitze at 2660 m a.s.l. (blue marker).

Moreover reliability of the data and coverage of the year 2022 were criteria for the selection. The type of measurement device used at the sites is either an sglux ERYCA broadband radiometer (site acronyms with 4 letters), a BTS2048-UV-S-WP spectroradiometer (site acronyms with 2 letters except for DO) and a Bentham DTM300 double monochromator at Dortmund (DO). The measurement devices are usually calibrated once a year with uncertainties of $\pm4\%$ (spectral devices, 2 letter acronyms) and $\pm10\%$ (broadband radiometers, 4 letter acronyms), respectively, where all calibrations are traceable to Physikalisch-Technische Bundesanstalt (PTB). Measurements of the UV Index were recorded every minute with the broadband devices, whereas the spectral instruments are logging a value every 2 or 6 minutes depending on the measurement site. The comparison with modelled data was then performed matching the timeline of satellite cloud information, which is available every 15 minutes, by using the ground measurements that were closest in time to the satellite recording (maximum time difference: 3 minutes).

Since the calculation of the CMF is associated with significant uncertainties for low solar elevations, further analysis is conducted with data from solar elevations of 20° and higher. As the UV Index is small for low solar elevations (UVI < 2) anyway, the increased uncertainty in the modelled UV Index maps for this regime is insignificant.

2.2 Comparison of the modelled UV Index to ground measurements

When comparing satellite-derived to ground-measured UV Index, there can be discrepancies due to various reasons. On the one hand there are uncertainties in both datasets, for example in the ground-based measurements due to calibration uncertainties (as mentioned above) or pollution of the detector input optics. The accuracy of the satellite-derived UV Index values, which are mainly determined by radiative transfer model calculations, is strongly dependent on the quality of the model input param-

acronym	location	m a.s.l.
TODO	Todendorf	5
ZIRC	Zirchow	30
LI	Lindenberg	114
SZ	Salzgitter	90
MP	Melpitz	85
DO	Dortmund	104
SCHA	Kassel	317
GOER	Görlitz	238
FIBG	Fichtelberg	1215
ANDE	Andernach	76
THOL	Tholey	386
WAMU	Waldmünchen	499
MB	Munich/Neuherberg	495
CHIM	Chieming	551
HP	Hohenpeißenberg	977
FRHA	Friedrichshafen	405
ZS	Schneefernerhaus	2660
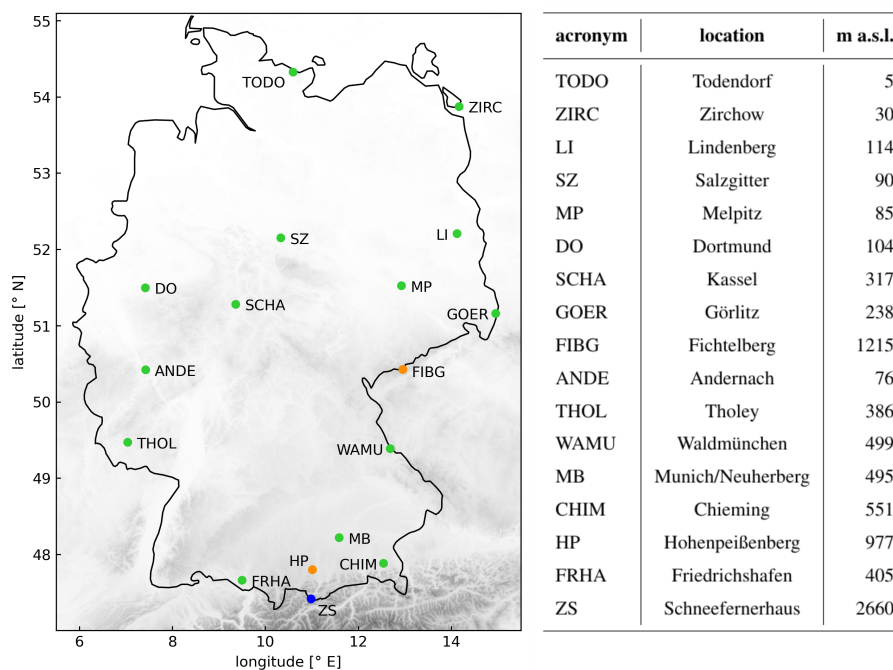
Figure 1. Locations of the measurement sites in Germany with low (green), mid (orange) and high (blue) altitude sites (left) and table of sites (right) with height above sea level and sorted from north to south

eters used. For the near-real-time UV Index map calculations presented here, these parameters are forecasted ozone, albedo and Angstrom β data from CAMS with a resolution of approximately 28 km x 45 km. The averaging over the larger pixel size is introducing higher uncertainties, especially when considering the albedo for mountainous areas with a highly variable topography. Moreover, uncertainties of the satellite products (SEVIRI images at 600 nm and the cloud mask) used in the CMF

95 calculation reduce the accuracy of the modelled UV Index maps for cloudy conditions. A discussion of the impact of different error sources on the modelled UV Index maps is given in Schenzinger et al. (2023). On the other hand satellite-derived and ground-measured UV Index values specify the same physical quantity, but for different spatial scopes. The satellite-derived map value represents an average over the pixel, whereas the ground measurement is strongly dependent on very localized conditions of albedo and clouds (especially for broken cloud conditions). Moreover nearby obstacles or the horizon (especially in

100 mountainous areas) have an impact on the ground measurements. These localized and often time dependent (clouds, albedo) effects can not easily be taken into account when modelling UV Index maps. Nevertheless, for cloudless conditions and areas with a homogeneous topography the comparison between modelled UV Index maps and ground-based measurements is expected to work well.

For the following statistical evaluations, the ground measurements with a maximum time difference of 3 minutes to the

105 satellite data acquisition were compared with the corresponding values from the modelled near-real-time UV Index map by selecting those pixels that contain the locations of the ground stations.

Table 1. Number of data points, mean and standard deviation (std) of the differences of modelled UVI to measured UVI and correlation coefficient (corr) of measured UVI to modelled UVI for clear, cloudy and all sky conditions

site	data points		mean			std			corr		
	clear	cloud	clear	cloud	all	clear	cloud	all	clear	cloud	all
TODO	3208	5878	-0.101	-0.404	-0.297	0.290	0.595	0.528	0.984	0.925	0.944
ZIRC	2978	6088	0.054	-0.242	-0.145	0.343	0.529	0.496	0.977	0.927	0.945
LI	2394	4188	-0.374	-0.654	-0.552	0.466	0.703	0.642	0.976	0.927	0.944
SZ	3117	5999	-0.180	-0.535	-0.413	0.364	0.718	0.643	0.979	0.918	0.933
MP	3206	5939	-0.284	-0.592	-0.484	0.444	0.685	0.629	0.972	0.935	0.942
DO	3236	5520	-0.134	-0.422	-0.315	0.306	0.599	0.529	0.986	0.932	0.952
SCHA	1028	2392	0.080	-0.251	-0.151	0.400	0.638	0.596	0.974	0.903	0.929
GOER	3527	6005	0.040	-0.318	-0.185	0.389	0.649	0.593	0.977	0.907	0.938
FIBG	1615	6829	-0.051	-0.247	-0.210	0.322	0.710	0.658	0.983	0.917	0.930
ANDE	3788	5900	-0.179	-0.513	-0.383	0.415	0.732	0.648	0.981	0.922	0.944
THOL	3555	6206	0.079	-0.262	-0.138	0.352	0.602	0.550	0.983	0.941	0.956
WAMU	3041	6781	0.098	-0.231	-0.129	0.455	0.737	0.680	0.973	0.909	0.932
MB	4049	5705	-0.149	-0.441	-0.320	0.364	0.659	0.574	0.985	0.929	0.959
CHIM	4866	5203	-0.143	-0.377	-0.264	0.475	0.612	0.562	0.979	0.935	0.966
HP	4068	5704	-0.111	-0.323	-0.235	0.411	0.744	0.636	0.982	0.915	0.954
FRHA	5510	4608	0.107	-0.236	-0.049	0.464	0.558	0.537	0.976	0.927	0.966
ZS	3540	6540	-0.452	-0.676	-0.597	0.759	1.465	1.267	0.957	0.740	0.854

The greatest temporally variable influence of all atmospheric parameters on the UV Index is cloud cover. So for the following analysis the dataset was divided into values measured and calculated under clear sky conditions and those under cloudy conditions. The filtering was based on the satellite product cloud mask (CLM), where the pixel value classified the data point 110 as cloudless or cloudy.

For the statistical comparisons, the difference between the UV Index from the calculated maps (modelled UVI) and ground measurements (measured UVI) was determined and mean and standard deviation (σ, std) were calculated for these distributions. Moreover the correlation coefficient (corr) for measured UVI to modelled UVI was computed (see Table 1) for clear sky and cloudy sky conditions as well as for the whole (all sky) dataset.

115 The distributions of the difference modelled UVI to measured UVI for clear and cloudy sky conditions are shown in Fig. 2. Systematic differences in the histograms are clearly evident when comparing clear sky conditions (blue) and cloudy conditions (grey) for each station. For cloud cover, the standard deviation is larger, and consequently, the correlation coefficient is smaller compared to the clear sky case (see Table 1). Additionally, the mean values of the distributions for cloudy conditions are slightly shifted towards negative UVI differences, whereas for clear sky conditions they are closer to zero.
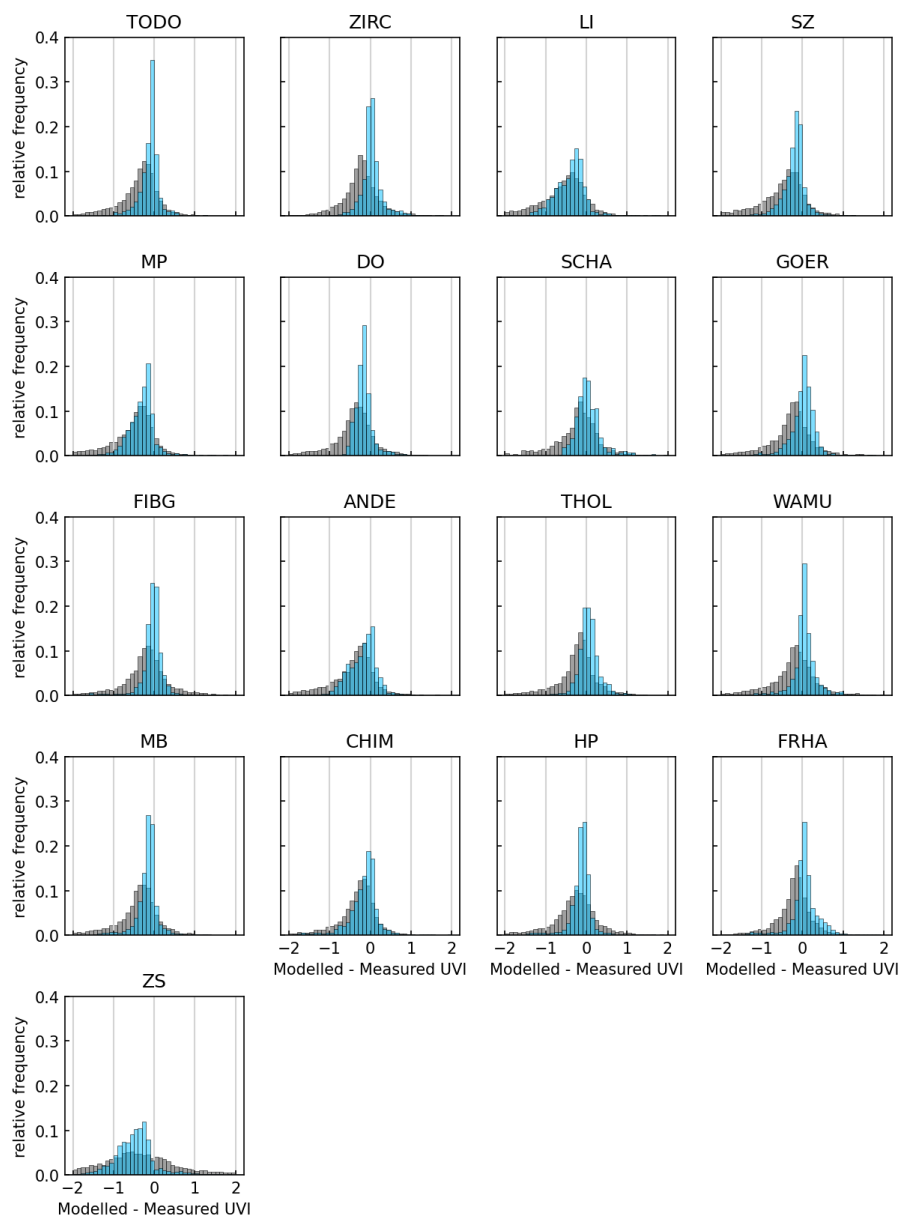
Figure 2. Histograms of the differences from modelled to measured UVI for clear sky (blue) and cloudy (grey) conditions for all ground sites

120   The correlation of measured UVI to modelled UVI for clear sky conditions is illustrated in Fig. 3 and for cloudy conditions in Fig. 4. Naturally in both cases the density of data points is highest for low UVI following the diurnal and annual pattern of the UV Index. For all stations the spread of data points is smaller in the clear sky case compared to the cloudy one, which is also reflected in the correlation coefficients (see Table 1).
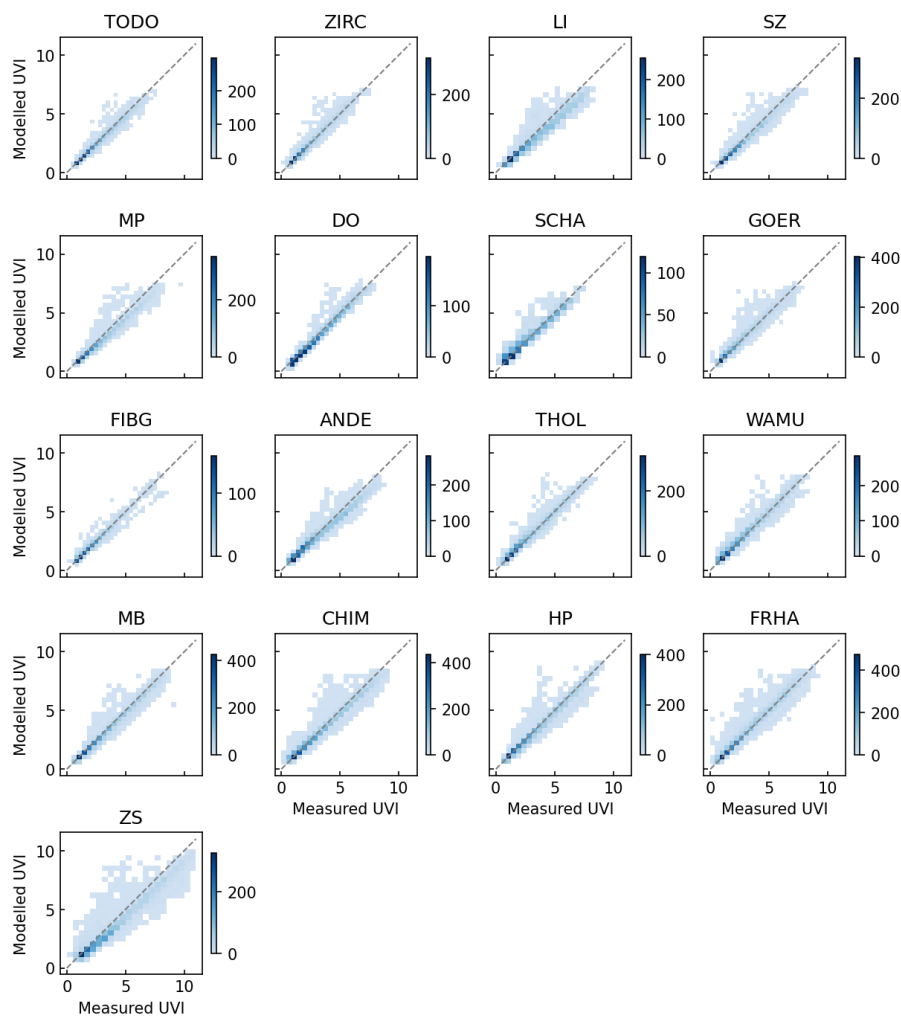
Figure 3. Correlation of measured UVI to modelled UVI for clear sky conditions for all ground sites; colours of the colour bar indicate the density of data points

The percentage of UVI differences (modelled minus measured UVI) within the ranges ±0.5 UV Index (U0.5) and ±1.0 UV In-

125 dex (U1.0) is given in Table 2 for clear sky and all sky conditions together with the average percentages across all stations. In the clear sky case the average for U0.5 is almost 83% and for U1.0 more than 95%, whereas in the all sky case the numbers drop to 69% (U0.5) and 87% (U1.0) due to increasing discrepancies between modelled and measured UV Index values for cloudy conditions.

A similar approach for calculating UV Index maps for Europe was presented in Kosmopoulos et al. (2021), where satellite

130 data from MSG was utilized for cloud analysis and then combined with ozone, aerosol, and ground albedo data as input parameters for a solar irradiance lookup table to compute near-real-time UVI maps. A comparison of the so called UVIOS
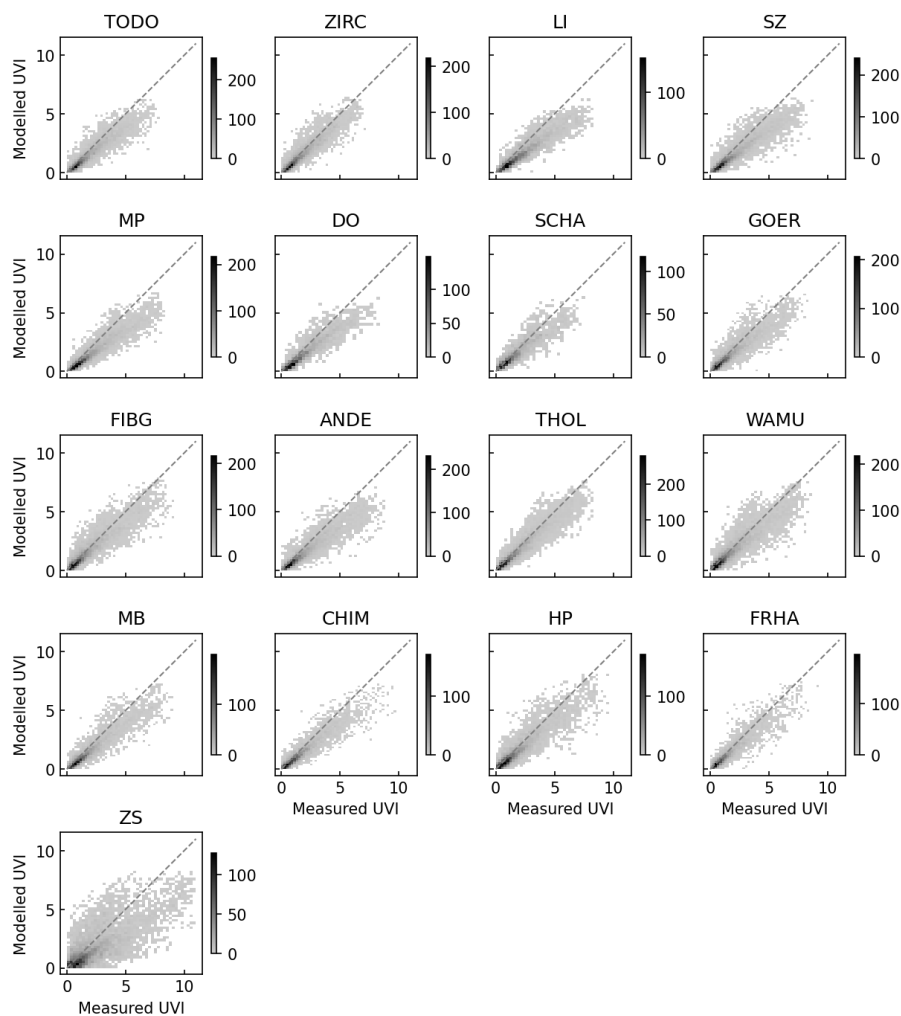
Figure 4. Correlation of measured UVI to modelled UVI for cloudy conditions for all ground sites; colours of the colour bar indicate the density of data points

(UV Index Operating System) model with measurements from 17 European ground stations for the year 2017 examined in Kosmopoulos et al. (2021) shows a good agreement with the study presented here for cloudless conditions. In the case of cloud cover, however, a comparison of the results of both studies is not meaningful as cloudiness (amount and main patterns) will differ between the respective years (2017 and 2022).

Table 2. U0.5 and U1.0 of the difference of modelled UVI to measured UVI and average of U0.5 and U1.0 across all stations

site	all		clear	
	U0.5	**U1.0**	**U0.5**	**U1.0**
TODO	73.79	90.72	91.24	98.66
ZIRC	77.52	93.86	91.03	98.39
LI	52.54	81.91	61.99	91.81
SZ	64.92	85.76	85.79	96.79
MP	60.48	85.10	72.40	95.13
DO	69.01	89.37	85.58	97.86
SCHA	74.21	89.94	89.20	96.21
GOER	75.50	90.12	90.50	96.60
FIBG	71.17	88.00	93.00	96.78
ANDE	65.72	87.26	76.35	96.86
THOL	78.68	91.93	91.20	98.23
WAMU	71.84	88.05	86.58	95.23
MB	73.21	89.42	89.28	96.37
CHIM	75.53	90.71	83.11	93.94
HP	74.27	89.36	90.34	95.38
FRHA	79.52	93.20	82.65	94.57
ZS	37.23	66.41	46.95	83.42
average	69.13	87.71	82.78	95.42

3 Discussion

Next we analyse the peculiarities of the results in Table 1 and Table 2 with regards to clear sky and cloudy conditions and the impact of topography. Finally we discuss potentially beneficial combinations of ground-based measurements and modelled UV Index maps.

3.1 Clear sky conditions

The overall agreement of the clear sky model with the ground measurements is quantified in terms of the mean and standard deviation of the distribution of UVI differences (modelled UVI - measured UVI) (see Table 1). Considering the mean values in the clear sky case, which range from -0.452 (ZS) to 0.107 (FRHA), no overall bias of the model is detected. These deviations of the mean value from zero are attributed to calibration uncertainties of the ground measurements as well as to pollution of the measurement devices. Moreover, uncertainties in the clear sky model are introduced by using forecast data from CAMS (ozone, albedo, Angstrom β) with a relatively coarse resolution of 0.4° (approximately 28 km x 45 km) as input for the LUT
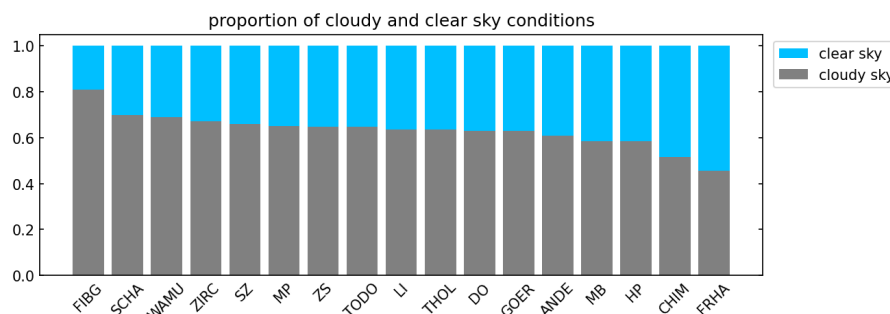
Figure 5. Proportion of measurements with cloudy (grey) and clear sky (blue) conditions for each ground station for the year 2022

interpolation. Especially in mountainous terrain with a highly variable topography the rough granularity of model input data is leading to higher uncertainties. This effect becomes apparent, when comparing the statistical parameters of the high mountain station Schneefernerhaus (ZS) with the results of other sites (see Fig. 2 and 3). In each case, the other stations exhibit more

150 favourable statistics than ZS (see Table 1 and Table 2).

3.2 Cloudy conditions

Especially with temporally variable cloud cover, it becomes apparent that due to the relatively coarse temporal (15 minutes) and spatial resolution (0.06°, 4 km x 7 km) of cloud information used for CMF calculation and cloud detection, there are larger discrepancies between ground measurements and modelled UV Index for cloudy conditions. This results in larger standard

155 deviations in the difference between modelled and measured UVI (see Fig. 2). On average, the model is underestimating the UVI in the presence of clouds for all stations in the range of -0.231 UVI (WAMU) up to -0.676 UVI (SZ) and also the correlation coefficients are decreasing (see Table 1) compared to the cloudless case.

When assessing the concordance between modelled and measured UV Index values across all sky conditions (both clear and cloudy), the uncertainty is considerably influenced by the climatology of cloudiness. Hence, Fig. 5 illustrates the proportion of

160 measurements with and without cloud cover at each station throughout the year 2022. Across the majority of sites, the proportion of cloudy measurements falls within the range of 60% to 65%. Consequently, for these stations, the impact of cloudiness on the uncertainty of the whole dataset (see column 'all' in Table 1) is quite similar. At Fichtelberg (FIBG), approximately 80% of the measurements were classified as cloudy, resulting in a standard deviation $\sigma = 0.658$ of the all sky UVI difference that is close to the corresponding value for cloudy sky scenarios ($\sigma = 0.710$). In contrast, the standard deviation for the clear

165 sky UVI difference in FIBG is significantly smaller with $\sigma = 0.322$. Friedrichshafen (FRHA) is the only site with a majority of clear sky measurements (5510 compared to 4608 cloudy sky measurements), but this prevalence (55% versus 45%) is too small to have a significant impact on the statistics of the all sky distribution.

Measured data from the ground stations Munich/Neuherberg (MB) and Hohenpeißenberg (HP) are suitable for comparisons due to their relatively close proximity of approximately 50 km linear distance. Nevertheless, for the Munich/Neuherberg sta-

170 tion situated at the northern outskirts of the city, higher Aerosol Optical Depth (AOD) levels are anticipated in comparison to Hohenpeißenberg, which is located in a rural area south-west of Munich. Moreover, the measurement station at Hohenpeißenberg is located approximately 500 m higher than the station in Munich/Neuherberg. So the ground measurements of MB are expected to be a bit lower than those from HP for clear sky conditions. In Fig. 6, measured and modelled UVI data from both stations are compared on days with partly cloud cover. The impact of clouds on ground measurements is clearly visible in

175 the diurnal variation of the UVI (top row). On May 31, 2022 both stations were affected by clouds approaching from the east (since MB is affected by cloudiness earlier in the day than HP) and on June 4, 2022, Hohenpeißenberg was less affected by cloud cover in the forenoon than the station in Munich/Neuherberg. This is also evident in the respective middle graphs, where green and blue dots are representing times with cloud cover according to the cloud mask. The ratios of measurements at MB to HP and modelled UVI at MB to HP do match quite well (red and orange lines), with only small deviations due to higher

180 uncertainties in the model calculations under cloudy conditions. The UVI difference of model to measurement for both sites is depicted in the bottom row and shows a good agreement especially for clear sky conditions of about 0.6 UVI and even for cloudy conditions most of the UVI differences are within 1 UVI.

In Fig. 7 a day (2022-10-12) with clouds in the vicinity of site Chieming (CHIM) is illustrated to show the limitations of the model due to the filtering in clear and cloudy situations via the satellite product cloud mask. When comparing the measured

185 UVI (green) to the clear sky model (blue) it is obvious that the ground measurements were affected by clouds during the whole day. Also the cloud mask is indicating clouds (white areas in the right timeline) to the east and the north of the site, nevertheless the pixel corresponding to the site location (red dot) is showing cloudless conditions up to 10:00 UTC. So for the model calculation cloudless conditions are assumed until 10:00 UTC, leading to a vast overestimation of the model (orange) compared to the actual measurements (green) and therefore to an increased UVI difference (red stars) in the range of 0.5 UVI

190 up to 1.7 UVI. After 10:00 UTC the cloud mask is indicating cloud cover also for the pixel of CHIM, thus the application of the CMF is decreasing the modelled UV Index resulting in a smaller UVI difference of about 0.5 UVI. In this case the sun, positioned to the east of the site in the forenoon, was obstructed by clouds in neighbouring pixels. Due to the filtering of the site pixel as unclouded, these data are increasing the standard deviation of the cloudless distribution of the UVI differences.

Of course, misleading filtering also impairs the statistics of the distribution for cloudy conditions, e.g. for broken cloud

195 situations, where the CLM is indicating a cloud for the pixel of the site while the direct sun may not be affected by clouds at all. For such conditions even an enhancement of the measured UVI compared to the clear sky expectation is possible (Pfister et al. (2003), Calbó et al. (2005)).

3.3 Impact of the topography

Most of the stations of the German Solar Monitoring Network used for this study (see Fig. 1) are located below 600 m a.s.l.

200 (see Fig. 1). Two sites, Hohenpeißenberg (HP, 977 m a.s.l.) and Fichtelberg (FIBG, 1215 m a.s.l.), are situated in the low mountain range and the high alpine station Schneefernerhaus (ZS) is positioned at 2660 m a.s.l.. When comparing the statistical parameters of HP and FIBG in Table 1 and U0.5 and U1.0 in Table 2 to the values of low altitude sites, no significant variation can be found, however this is not true for the site Schneefernerhaus. The distributions of the UVI differences from the site
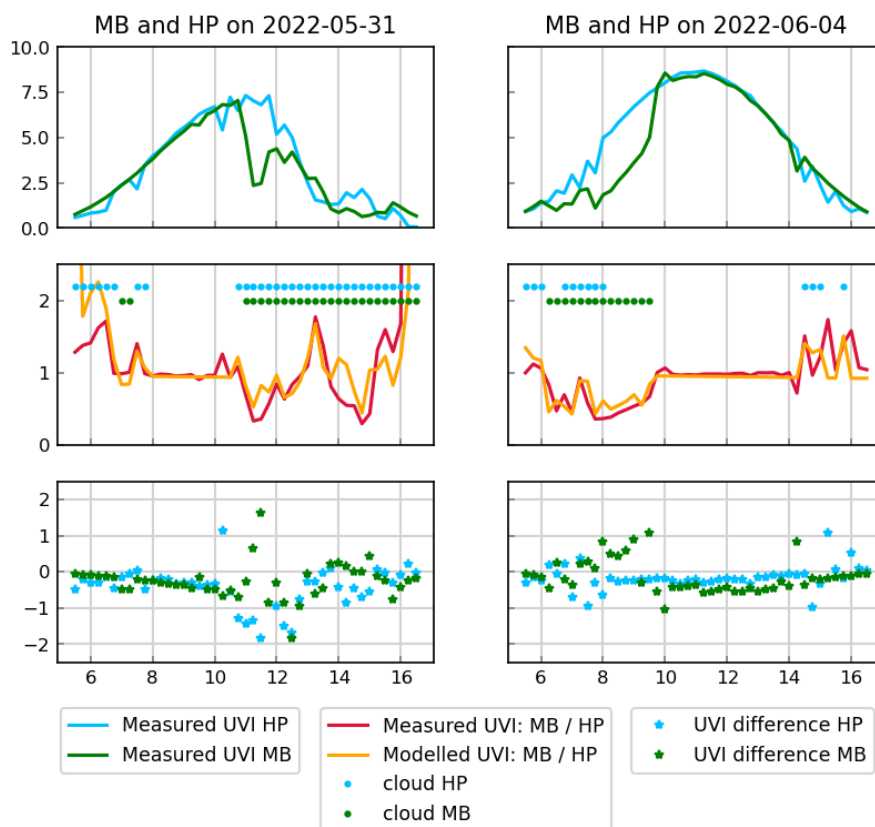
Figure 6. Comparison of MB and HP on days with partly clouds: measured UV Index from MB and HP (top row, left legend), ratio of measurements MB / HP with cloud filtering for both sites (middle row, middle legend), difference of modelled UVI and measured UVI for both sites (bottom row, right legend)

Schneefernerhaus (ZS) show the largest standard deviations and biggest shifts of the mean value from zero (see Table 1)
205 compared to the results of all other stations for clear sky as well as cloudy conditions and consequently also for the analysis of the all sky dataset. Accordingly, the correlation coefficients are smaller for site ZS, not only but especially for cloudy conditions with 0.740 compared to the correlation coefficients of the other stations, all of which are above 0.9. Also the percentages of U0.5 and U1.0 are considerably lower than those from the other sites (see Table 2).

This is attributed to the pronounced topography in the mountains, which is characterized by spatially small-scale variable
210 albedo and cloud situations. Under such conditions, the predicted albedo data from CAMS, which provides an average value over an area of about 28 km x 45 km (pixel resolution 0.4°), and the cloud information derived from satellite images, available at a resolution of approximately 4 km x 7 km (0.06°), are not representative for the actual conditions at the site.
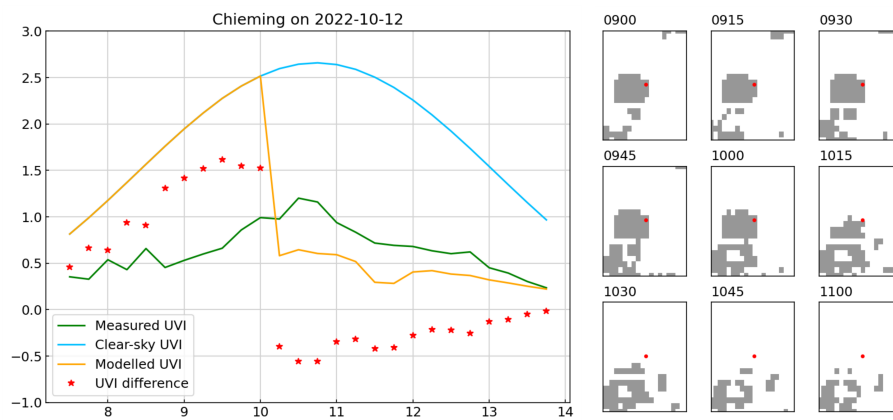
Figure 7. Comparison of measured (green) and modelled (orange) UVI at the site Chieming (CHIM) for day 2022-10-12 (left) and a selection of CLM (cloud mask) details (right) to illustrate the cloud situation in the vicinity of the site

3.4 Combination of ground-based measurements and modelled UV Index maps

There are beneficial prospects in integrating ground-based measurements, which provide real-time information about the cur-

215 rent UV radiation levels in the vicinity of a site, with modelled UV Index maps based on satellite imagery. While ground-based measurements offer continuous data, modelled UV Index maps provide extensive coverage across larger areas but only at specific time intervals.

First modelled data for cloudless sky conditions can be used for quality control of the ground-based measurements. When comparing the ratio of measured UVI to the corresponding pixel of the modelled UV Index maps, periods with larger deviations

220 can help to identify problems with the ground-based measurement devices. In particular, if the deviations only occur in the data of one station, this is a strong indication of possible contamination of the detectors or some form of defect.

Furthermore, modelled UV Index maps can provide climatological data, particularly for regions that are not in close proximity to a ground station. Maintaining a high density of ground stations is costly and time consuming. Receiving near-real-time measurements from SEVIRI / MSG also involves additional infrastructure and processing, but the effort is much lower com-

225 pared to maintaining a ground-based network.

By using geospatial interpolation techniques, area covering UV Index information can be gained from ground-based measurements (Schmalwieser and Schauberger (2001), Duguay (1995)). Nevertheless, without area-wide cloud information these UV Index maps are associated with large uncertainties. So the goal is to combine both datasets to benefit on the one hand from the accuracy of measured UV levels at the ground and on the other hand from the area-wide coverage provided by

230 satellite-based UV Index maps.

The idea is to utilize the ratio between simultaneously measured and modelled UV Index values at ground station locations as supporting points for a spatial interpolation to create a comprehensive correction map for each modelled UV Index map. This approach was tested for clear sky conditions by selecting days with very low cloud coverage in the area of Germany. Next

for each point in time (15 minute intervals) the subset of clear sky data from all 17 sites was filtered via the cloud mask. Then
235 the ratio of these data points to the corresponding pixel values of the UV Index maps was analysed. While most of the data
points lie within 0.8 to 1.2, there are some outliers that are attributed to uncertainties in the model calculation due to forecasted
and spatially coarse input parameters or to faulty cloud filtering (compare Fig. 7). So the ratio data points were limited to the
range from 0.8 up to 1.2 and then geostatistically interpolated to obtain correction maps for the UV Index maps. The Kriging
interpolation method (Oliver and Webster (1990), Meng et al. (2013)) was initially evaluated, for which the spatial correlation
240 of the data points is crucial. However, the correlation of a maximum of 17 clear sky data points, widely distributed in the area
of Germany, proved insufficient to yield meaningful results with this method.

Therefore, the RBFInterpolator method (Radial Basis Function Interpolator) from the Python SciPy package was then used
for calculating the spatial distribution. This method is suitable for interpolating multidimensional data points. The method is
based on radial basis functions (RBF) with a linear kernel, whose value depends only on the distance from the centre of the
245 function. A deliberately simple approach with a plausible distance weighting was chosen for the calculation of the spatial
distribution, as it will be shown in the following that the fundamental issue does not lie in the details of the spatial interpolation
method.

The results for July 17, 2022 are illustrated in Fig. 8, showing the course of measured and modelled UV Index values
per station, along with the resulting ratios (upper section). In the representation of the ratios, the data points for cloudless
250 conditions are depicted in black. These values form the basis for the calculation of correction maps (lower part of the figure)
through spatial interpolation at individual points in time.

On this day, spatial interpolation can be performed using measured values from 16 ground stations throughout the day,
although never all stations were unclouded simultaneously (see black points in the interpolated correction factor maps). Con-
sidering the timeline of correction factor maps (lower part of Fig. 8), the spatial distribution is varying strongly with time,
255 showing the effect of missing data points (grey dots). For example at 9:00 UTC the station Salzgitter (SZ) is obstructed by
clouds and therefore missing in the calculation of the correction map, leading to a correction factor of slightly below 1 in the
northern part of Germany, while before and after that the correction is bigger than 1 in that area. The data from Todendorf
(TODO) are also used only intermittently, resulting in an inhomogeneous temporal pattern of correction maps. In comparison
to the model, the data from Friedrichshafen (FRHA) are consistently lower at approximately 0.9 but remain constant through-
260 out the day. The closely located stations Munich/Neuherberg (MB), Chieming (CHIM) and Hohenpeißenberg (HP) all show a
similar correction factor that remains constant throughout the day, which increases the confidence in the correction factors in
the vicinity of these stations.

In essence, it is evident that each ground station has the potential to exert a significant influence on the correction maps,
and a variable number of used data points for interpolation results in timely variable corrections. This raises the question of
265 how and at what frequency corrections should judiciously be applied. Uncertainties arise both in ground measurements, which
typically undergo post hoc verification and potential correction, and in the input parameters for the model calculation, initially
provided as forecast values and only later available in higher quality through measurements.
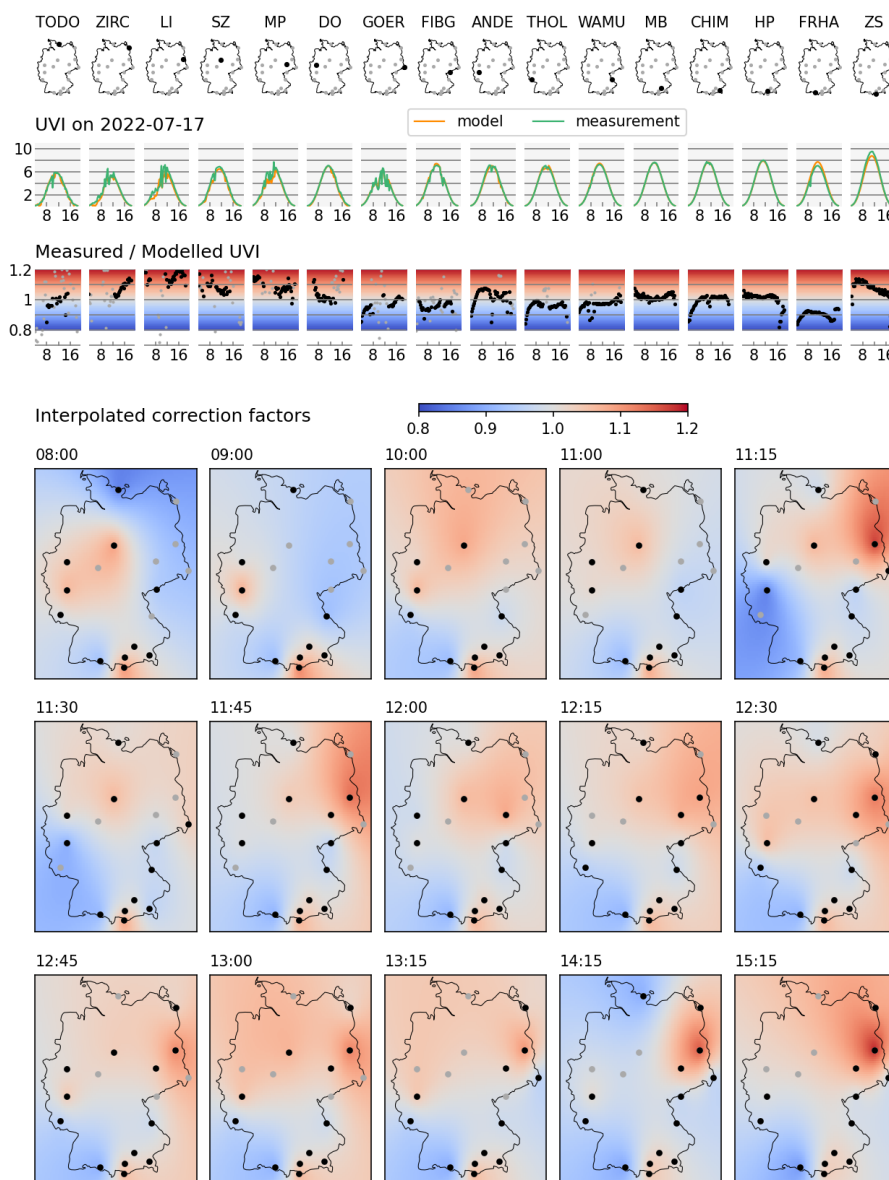
Figure 8. From top to bottom: Location of the ground station, daily course of measured and modelled UV Index, ratio of measurement to model, and spatially interpolated correction factors for July 17, 2022

When considering the combination of ground-based measurements with modelled UV Index maps for cloudy conditions the shortcomings become even worse. When the intra pixel variability of clouds becomes significant, ground-based data can vary from very low UV Index to values even higher than the clear sky model expectations. However, the modelled UV Index, which is relying on the information of a pixel to be cloudy, will always be smaller than the clear sky model expectation.

This circumstance is the main factor leading to the enlarged standard deviations of the UVI difference for cloudy conditions compared to the clear sky case (see Table 1). In principle for broken cloud conditions satellite derived UV Index maps lack the representativeness for ground-based measurements and vice versa.

4   Conclusions

In this study, the method to calculate near-real-time UV Index maps (Schenzinger et al. (2023)), that is used operationally in the framework of the Austrian UV Monitoring Network, is employed to calculate UV Index maps for the area of Germany. Clear sky UV Index maps are retrieved from a pre-calculated lookup table of erythemally weighted UV radiation by employing forecasted data of total ozone column, albedo and aerosol optical depths from the CAMS global model forecast. To incorporate the effects of clouds in the model, a cloud modification factor (CMF) is derived from SEVIRI imagery, that is recorded every 15 minutes onboard the MSG satellite.

With this method, almost 22.000 UV Index maps of Germany have been calculated for the year 2022. Ground-based measurements of 17 stations of the German Solar Monitoring Network where then compared to the corresponding pixel value of the modelled maps. Statistical analysis of the UVI differences (modelled minus measured UVI) show a good agreement between model and measurements for clear sky conditions with almost 83% of all clear sky UVI differences being within 0.5 UVI and 95% within 1.0 UVI (see Table 2). Also the correlation between measured and modelled UVI is higher than 0.95 for all sites (see Table 1).

For cloudy conditions the statistics worsen, with only 69% of the UVI differences being within 0.5 UVI and 87% within 1.0 UVI (see Table 2). This is due to the uncertainties arising from the cloud information retrieval from satellite data, which can not properly represent the actual cloud situation affecting the solar radiation at the location of the ground site. Especially for broken cloud conditions, the pixel size of 4 km x 7 km (0.06° resolution) of the satellite data is insufficient to reproduce the effects of small scale clouds.

Not only clouds but also highly variable topography (e.g. in mountainous regions) is adding to the uncertainties in the modelled UV Index maps. The statistics of the site Schneefernerhaus (ZS), located at 2660 m a.s.l. in the alpine region, are worse than the corresponding values of all the other sites and for all considered conditions (clear, cloudy and all sky). With a highly variable small-scale topography, albedo predictions from CAMS with a pixel size of approximately 28 km x 45 km (0.4° resolution) can not represent the actual albedo situation influencing measurements at the location of the high alpine site.

So, for cloudy conditions (especially broken clouds) and small-scale variable topography satellite derived UV Index maps lack the representativeness for ground-based measurements and vice-versa. Nevertheless, there are beneficial prospects in combining ground-based measurements and modelled UV Index maps. Ground-based measurements provide continuous UV radiation levels at the ground, but restricted in their significance to the vicinity of a site, whereas modelled UV Index maps based on satellite imagery offer extensive area coverage but only at specific time intervals.

The possibility of integrating both datasets via a correction factor map based on the ratio of modelled UVI to measured UVI was tested for clear sky conditions. By spatially interpolating the ratio of clear sky modelled to measured UVI for each

305 point in time (15 minute interval), correction factor maps with values from 0.8 to 1.2 were generated for days with low cloud coverage. The case study presented for July 17, 2022 shows that the spatial distribution of the correction factor maps is varying strongly with time because the geostatistical interpolation is sensitive to the number of supporting points. With a loose cloud field passing through, the data of a site are only used intermittently, leading to an inhomogeneous correction factor throughout the day. Moreover, each ground station has the potential to exert a significant influence on the correction maps (see Fig. 8). If

310 considering a correction for cloudy conditions all the above mentioned discrepancies add to the problem. This leaves us with the question of how and at what frequency corrections should judiciously be applied. Naturally, the answer to this question depends on the specific application. So, for the improvement of near-real-time UV Index maps a different approach for the correction may be expedient than for analysing the data in retrospect. Uncertainties emerge in both ground measurements, commonly subjected to post hoc validation and potential adjustments, and in the input parameters for model calculations,

315 initially supplied as forecast values and later refined to higher quality through subsequent measurements.

To further explore possible synergies of ground-based measurements and satellite derived maps more investigations on the proper methods to combine them are planned.

Author contributions. BK processed the UV Index measurements of the German Solar Monitoring Network, compared them with model results, derived the correction factor maps and was responsible for quality assurance. MS calculated the clear-sky lookup table. VS designed

320 and implemented the CMF algorithm. The manuscript and figures were drafted by BK, with all authors contributing to its final state.

Competing interests. The authors declare no competing interests.

Acknowledgements. The authors thank Sebastian Lorenz of the German Federal Office for Radiation Protection (BfS) for providing most of the ground data of the German Solar Monitoring Network (including preprocessing and quality control of all ground data used in this study) and for valuable discussions.

325 The authors thank the Meteorological Observatories Lindenberg and Hohenpeißenberg of the German National Meteorological Service (DWD) for providing ground measurements of the stations Lindenberg and Hohenpeißenberg, the Federal Institute for Occupational Safety and Health (BAuA) for providing ground measurements of the station Dortmund and the Leibniz Institute for Tropospheric Research (TRO-POS) for providing ground measurements of the station Melpitz.

The authors thank the German Federal Office for Radiation Protection (BfS) and the German Federal Ministry for the Environment, Nature

330 Conservation, Nuclear Safety and Consumer Protection (BMUV) for supporting this study.

The Austrian UV network is supported by a grant from the Federal Ministry for Climate Action, Environment, Energy, Mobility, Innovation and Technology (BMK).

This publication uses Copernicus Atmosphere Monitoring Service Information [2023]; neither the European Commission nor ECMWF is responsible for any use that may be made of the information it contains.

References

Calbó, J., Pagès, D., and González, J.-A.: Empirical studies of cloud effects on UV radiation: A review, Reviews of Geophysics, 43, https://doi.org/10.1029/2004RG000155, 2005.

CAMS: CAMS global atmospheric composition forecasts, https://ads.atmosphere.copernicus.eu/cdsapp#!/dataset/cams-global-atmospheric-composition-forecasts?tab=overview, last accessed 2022/12/12, 2021.

Duguay, C. R.: An approach to the estimation of surface net radiation in mountain areas using remote sensing and digital terrain data, Theoretical and Applied Climatology, 52, 55–68, https://doi.org/10.1007/BF00865507, 1995.

Emde, C., Buras-Schnell, R., Kylling, A., Mayer, B., Gasteiger, J., Hamann, U., Kylling, J., Richter, B., Pause, C., Dowling, T., and Bugliaro, L.: The libRadtran software package for radiative transfer calculations (version 2.0.1), Geoscientific Model Development, 9, 1647–1672, https://doi.org/10.5194/gmd-9-1647-2016, 2016.

EUMETSAT: MSG Meteorological Products Extraction Facility Algorithm Specification Document, EUMETSAT, doc.No. EUM/MSG/SPE/022, Issue v7B e-signed, 2015.

EUMETSAT: MSG Level 1.5 Image Data Format Description, EUMETSAT, doc.No. EUM/MSG/ICD/105, Issue v8 e-signed, 2017.

Gesch, D. B., Verdin, K. L., and Greenlee, S. K.: New land surface digital elevation model covers the Earth, Eos, Transactions American Geophysical Union, 80, 69–70, https://doi.org/10.1029/99EO00050, 1999.

Juzeniene, A., Brekke, P., Dahlback, A., Andersson-Engels, S., Reichrath, J., Moan, K., Holick, M. F., Grant, W. B., and Moan, J.: Solar radiation and human health, Reports on Progress in Physics, 74, 066 701, https://doi.org/10.1088/0034-4885/74/6/066701, 2011.

Kosmopoulos, P. G., Kazadzis, S., Schmalwieser, A. W., Raptis, P. I., Papachristopoulou, K., Fountoulakis, I., Masoom, A., Bais, A. F., Bilbao, J., Blumthaler, M., Kreuter, A., Siani, A. M., Eleftheratos, K., Topaloglou, C., Gröbner, J., Johnsen, B., Svendby, T. M., Vilaplana, J. M., Doppler, L., Webb, A. R., Khazova, M., De Backer, H., Heikkilä, A., Lakkala, K., Jaroslawski, J., Meleti, C., Diémoz, H., Hülsen, G., Klotz, B., Rimmer, J., and Kontoes, C.: Real-time UV index retrieval in Europe using Earth observation-based techniques: system description and quality assessment, Atmospheric Measurement Techniques, 14, 5657–5699, https://doi.org/10.5194/amt-14-5657-2021, 2021.

Lucas, R., McMichael, T., Smith, W., and Armstrong, B.: Solar Ultraviolet Radiation: Global burden of disease from solar ultraviolet radiation, WHO Environmental Burden of Disease Series, 13, 2006.

Mayer, B. and Kylling, A.: Technical note: The libRadtran software package for radiative transfer calculations - description and examples of use, Atmospheric Chemistry and Physics, 5, 1855–1877, https://doi.org/10.5194/acp-5-1855-2005, 2005.

Meng, Q., Zhijun, L., and Borders, B. E.: Assessment of regression kriging for spatial interpolation – comparisons of seven GIS interpolation methods, artography and Geographic Information Science, 40, 28–39, https://doi.org/110.1080/15230406.2013.762138, 2013.

Oliver, M. A. and Webster, R.: Kriging: a method of interpolation for geographical information systems, International journal of geographical information systems, 4, 313–332, https://doi.org/10.1080/02693799008941549, 1990.

Pfister, G., McKenzie, R. L., Liley, J. B., Thomas, A., Forgan, B. W., and Long, C. N.: Cloud Coverage Based on All-Sky Imaging and Its Impact on Surface Solar Irradiance, Journal of Applied Meteorology, 42, 1421 – 1434, https://doi.org/10.1175/1520-0450(2003)042<1421:CCBOAI>2.0.CO;2, 2003.

Schallhart, B., Blumthaler, M., Schreder, J., and Verdebout, J.: A method to generate near real time UV-Index maps of Austria, Atmospheric Chemistry and Physics, 8, 7483–7491, https://doi.org/10.5194/acp-8-7483-2008, 2008.

Schenzinger, V., Kreuter, A., Klotz, B., Schwarzmann, M., and Gröbner, J.: On the production and validation of satellite based UV index maps, Atmospheric Measurement Techniques Discussions, 2023, 1–26, https://doi.org/10.5194/amt-2023-188, 2023.

Schmalwieser, A. W. and Schauberger, G.: A monitoring network for erythemally-effective solar ultraviolet radiation in Austria: determination of the measuring sites and visualisation of the spatial distribution, Theoretical and Applied Climatology, 69, 221–229,

375   https://doi.org/10.1007/s007040170027, 2001.

Verdebout, J.: A method to generate surface UV radiation maps over Europe using GOME, Meteosat, and ancillary geophysical data, Journal of Geophysical Research, 105, 5049–5058, 2000.

Webb, A. R. and Engelsen, O.: Calculated Ultraviolet Exposure Levels for a Healthy Vitamin D Status, Photochem. Photobiol., 82, 1697, https://doi.org/10.1111/j.1751-1097.2006.tb09833.x, 2006.

380   Webb, A. R., Kift, R., Berry, J. L., and Rhodes, L. E.: The vitamin D debate: Translating controlled experiments into reality for human sun exposure times, Photobiol., 87, 741–745, https://doi.org/10.1111/j.1751-1097.2011.00898.x, 2011.

WHO/WMO: Global solar UV index : a practical guide, World Health Organization, a joint recommendation of the World Health Organization, World Meteorological Organization, United Nations Environment Programme, and the International Commission on Non-Ionizing Radiation Protection, 2002.